A&A 615, L16 (2018)
https://doi.org/10.1051/0004-6361/201833607

Astronomy & Astrophysics

LETTER TO THE EDITOR

Depletion of ^{15}N in the center of L1544: Early transition from atomic to molecular nitrogen?

K. Furuya[1], Y. Watanabe[2,3], T. Sakai[4], Y. Aikawa[5], and S. Yamamoto[6]

[1] Center for Computational Sciences, University of Tsukuba, 1-1-1 Tennoudai, 305-8577 Tsukuba, Japan
e-mail: furuya@ccs.tsukuba.ac.jp
[2] Division of Physics, Faculty of Pure and Applied Sciences, University of Tsukuba, Tsukuba, Ibaraki 305-8571, Japan
[3] Tomonaga Center for the History of the Universe, Faculty of Pure and Applied Sciences, University of Tsukuba, Tsukuba, Ibaraki 305-8571, Japan
[4] Graduate School of Informatics and Engineering, The University of Electro-Communications, Chofu, Tokyo 182-8585, Japan
[5] Department of Astronomy, The University of Tokyo, Bunkyo-ku, Tokyo 113-0033, Japan
[6] Department of Physics, The University of Tokyo, Bunkyo-ku, Tokyo 113-0033, Japan

Received 11 June 2018 / Accepted 7 July 2018

ABSTRACT

We performed sensitive observations of the $N^{15}ND^+$(1–0) and $^{15}NND^+$(1–0) lines toward the prestellar core L1544 using the IRAM 30 m telescope. The lines are not detected down to 3σ levels in 0.2 km s^{-1} channels of ∼6 mK. The non-detection provides the lower limit of the $^{14}N/^{15}N$ ratio for N_2D^+ of ∼700–800, which is much higher than the elemental abundance ratio in the local interstellar medium of ∼200–300. The result indicates that N_2 is depleted in ^{15}N in the central part of L1544, because N_2D^+ preferentially traces the cold dense gas, and because it is a daughter molecule of N_2. In situ chemistry is probably not responsible for the ^{15}N depletion in N_2; neither low-temperature gas phase chemistry nor isotope selective photodissociation of N_2 explains the ^{15}N depletion; the former prefers transferring ^{15}N to N_2, while the latter requires the penetration of interstellar far-ultraviolet (FUV) photons into the core center. The most likely explanation is that ^{15}N is preferentially partitioned into ices compared to ^{14}N via the combination of isotope selective photodissociation of N_2 and grain surface chemistry in the parent cloud of L1544 or in the outer regions of L1544, which are not fully shielded from the interstellar FUV radiation. The mechanism is most efficient at the chemical transition from atomic to molecular nitrogen. In other words, our result suggests that the gas in the central part of L1544 has previously gone trough the transition from atomic to molecular nitrogen in the earlier evolutionary stage, and that N_2 is currently the primary form of gas-phase nitrogen.

Key words. astrochemistry – ISM: clouds – ISM: molecules – ISM: individual objects: L1544

1. Introduction

Nitrogen is the fifth most abundant element in the universe. Our understanding of nitrogen chemistry in star-forming regions is limited compared to other volatile elements, such as carbon and oxygen. The dominant form of gaseous nitrogen in star-forming regions is unclear (e.g., Bergin & Tafalla 2007), while it is theoretically expected to be either atomic N or N_2 (e.g., Aikawa et al. 2005; Le Gal et al. 2014). One of the main limiting factors is that neither atomic N nor N_2 is directly observable in the cold and dense gas of star-forming regions. However, the N_2 abundance can be constrained indirectly by observing a proxy molecule N_2H^+ (e.g., Maret et al. 2006).

The observational and theoretical studies of nitrogen isotope fractionation in star-forming regions can help to constrain nitrogen chemistry. Nitrogen has two stable isotopes, ^{14}N and ^{15}N. The elemental abundance ratio $[^{14}N/^{15}N]_{elem}$ in the local interstellar medium (ISM) has been estimated to be ∼200–300 from the absorption line observations of N-bearing molecules toward diffuse clouds (Lucas & Liszt 1998; Ritchey et al. 2015). L1544 is a prototypical prestellar core located in the Taurus molecular cloud complex. In L1544, the $^{14}N/^{15}N$ ratio of several different molecules has been measured: $^{14}N_2H^+/N^{15}NH^+ = 920^{+300}_{-200}$, $^{14}N_2H^+/^{15}NNH^+ = 1000^{+260}_{-220}$ (Bizzocchi et al. 2013; Redaelli et al. 2018), $NH_2D/^{15}NH_2D > 700$ (Gérin et al. 2009), $CN/C^{15}N = 500 \pm 75$ (Hily-Blant et al. 2013b), and $HCN/HC^{15}N = 257$ (Hily-Blant et al. 2013a). Among the measurements, the significant depletion of ^{15}N in N_2H^+ is the most challenging for the theory of ^{15}N fractionation. In general, molecules formed at low temperatures are enriched in ^{15}N through gas-phase chemistry triggered by isotope exchange reactions (e.g., Terzieva & Herbst 2000). A ^{15}N-bearing molecule has a slightly lower zero-point energy than the corresponding ^{14}N isotopolog. This results in endothermicity for the exchange of ^{15}N for ^{14}N, which inhibits this exchange at low temperature enabling the concentration of ^{15}N in molecules. Astrochemical models for prestellar cores, which consider a set of nitrogen isotope exchange reactions, have indeed predicted that atomic N is depleted in ^{15}N, while N_2 (and thus N_2H^+) is enriched in ^{15}N (e.g., Charnley & Rodgers 2002). The model prediction clearly contradicts the observation of the N_2H^+ isotopologs in L1544. The ^{15}N depletion in N_2H^+ was recently found in other prestellar cores as well, such as L183, L429, and L694-2 (Redaelli et al. 2018). Furthermore, Roueff et al. (2015) recently pointed out the presence of activation barriers for some key nitrogen isotope exchange reactions, based on their quantum chemical calculations. Then ^{15}N fractionation

triggered by isotope exchange reactions may be much less efficient than previously thought (Roueff et al. 2015, but see also Wirström & Charnley 2018).

Another mechanism that can cause ^{15}N fractionation is photodissociation of N_2 (Heays et al. 2014). N_2 photodissociation is prone to self-shielding. Because $^{14}N^{15}N$ is much less abundant than $^{14}N_2$, $^{14}N^{15}N$ needs a higher column density of the ISM gas for self-shielding. This makes N_2 photodissociation an isotope-selective process. As a result, N_2 is depleted in ^{15}N, which is consistent with the observation of the N_2H^+ isotopologs in L1544. Isotope-selective photodissociation of N_2 is efficient only for limited regions where the interstellar UV radiation field is not significantly attenuated, however (Heays et al. 2014; Furuya & Aikawa 2018). The prestellar core L1544 has high density and A_V (>10 mag for a millimeter-dust continuum peak). Detection of carbon chain species, such as C_3H_2, however, may indicate that the interstellar UV radiation penetrates to moderate depth in L1544 (Spezzano et al. 2016). Then it is unclear whether the isotope-selective photodissociation of N_2 is at work in L1544, and how it affects the measurement of the $^{14}N/^{15}N$ ratio of N_2H^+.

In order to test the selective photodissociation scenario, we observed ^{15}N isotopologs of N_2D^+ toward prestellar core L1544. Compared with N_2H^+, N_2D^+ selectively traces colder and denser regions (i.e., core center) (Caselli et al. 2002a), where the attenuation of the interstellar UV radiation field is more significant. If the isotope-selective photodissociation of N_2 by the penetrating UV radiation is the cause of the ^{15}N depletion in N_2H^+, the $^{14}N/^{15}N$ ratio of N_2D^+ should be lower than that of N_2H^+ and be close to $[^{14}N/^{15}N]_{elem}$. Moreover, N_2D^+ is less optically thick than N_2H^+, which allows us to accurately evaluate the column density of the ^{14}N isotopolog and thus the $^{14}N/^{15}N$ ratio, although more sensitive observations are required for the detection of the ^{15}N isotopologs of N_2D^+ than those of N_2H^+.

2. Observations

We observed the $N^{15}ND^+(1–0)$, $^{15}NND^+(1–0)$, and $N_2D^+(1–0)$ transitions toward the prestellar core L1544 with the IRAM 30 m telescope at Pico Veleta on 2017 December 22–24. We tracked the L1544 continuum dust emission peak at 1.3 mm, where ^{15}N isotopologs of N_2H^+ were previously detected (Bizzocchi et al. 2010, 2013). The observed position is (α_{J2000}, σ_{J2000}) = ($05^h04^m17\overset{s}{.}21$, $25°10'42\overset{''}{.}8$) (Caselli et al. 2002a). The telescope pointing was checked every two hours by observing the continuum source 0439+360 near the target position and was ensured to be better than ±3″. The half-beam power width was 32″–33″.

We employed Eight Mixer Receiver (EMIR) E090 with dual polarization mode. The system noise temperatures were typically from 70 K to 130 K during the observation run. The $N^{15}ND^+(1–0)$ and $^{15}NND^+(1–0)$ transitions were observed simultaneously (Set 1), while the $N_2D^+(1–0)$ transition was observed with a different frequency setting (Set 2). The hyperfine components and their relative intensities of the $N^{15}ND^+(1–0)$ and $^{15}NND^+(1–0)$ transitions were experimentally studied by Dore et al. (2009), and they are listed in Table A.1. A frequency-switching mode was employed with a frequency offset of 7.35 MHz. We used eight Fourier transform spectrometer (FTS) autocorrelators with a bandwidth of 1820 MHz. The frequency resolution of 50 kHz corresponds to 0.2 km s^{-1} at 75 GHz. We integrated the spectrum for a total on-source time of 5.2 h for Set 1 and 0.4 h for Set 2. Two orthogonal polarizations were simultaneously observed, and are averaged together to produce the final spectrum. The main-beam temperature (T_{MB}) is derived by $T_a^* F_{eff}/B_{eff}$, where T_a^* is the antenna temperature, F_{eff} is the forward efficiency (95%), and B_{eff} is the main-beam efficiency (74%). The final rms noise is 2.3 mK in T_{MB} for $N^{15}ND^+(1–0)$, 2.1 mK for $^{15}NND^+(1–0)$, and 11 mK for $N_2D^+(1–0)$. The $N^{15}NH^+(1–0)$ and $^{15}NNH^+(1–0)$ transitions were also observed in Set 1. Both transitions were detected, and the obtained spectra are similar to those obtained in the framework of ASAI IRAM 30 m large program (De Simone et al. 2018; Lefloch et al. 2018), which observed the same object and the same position with the same velocity resolution, but employing wobbler-switching mode. We do not discuss the observations of the ^{15}N isotopologs of N_2H^+ in this work because they have been studied in detail in previous work (Bizzocchi et al. 2010, 2013; De Simone et al. 2018).

Table 1. Derived column density and $^{14}N/^{15}N$ ratio.

Species	N_{tot} (cm^{-2})	$^{14}N/^{15}N$
N_2D^+	$(5.4 \pm 0.3) \times 10^{12}$	–
$N^{15}ND^+$	$<7.0 \times 10^9$	>730
$^{15}NND^+$	$<6.5 \times 10^9$	>780

3. Results

The data were processed using the GILDAS software (Pety et al. 2005). The $N_2D^+(1–0)$ transition was clearly detected, while $N^{15}ND^+(1–0)$ and $^{15}NND^+(1–0)$ were not detected, as shown in Fig. 1. Line parameters for $N_2D^+(1–0)$ were estimated using the HFS routine implemented in CLASS. The derived total optical depth of the lines and the FWHM line width are 3.08 ± 0.19 and 0.406 ± 0.003 km s^{-1}, respectively. The main component of the $N_2D^+(1–0)$ transition (77.1096162 GHz), which has a fraction of 7/27 of the total line strength, is marginally optically thick (~0.8). We derived the total column density of N_2D^+ using Eq. (A1) of Caselli et al. (2002b), which is valid for optically thick emission. For the column density calculation, the excitation temperature (T_{ex}) was set to be 5 K, which was previously derived from $N_2H^+(1–0)$ and $N_2D^+(2–1)$ observations toward the same object and the same position (Caselli et al. 2002a; Crapsi et al. 2005). The parameters of the observed transitions were taken from the Cologne Database for Molecular Spectroscopy (Müller et al. 2001, 2005). The total column density of N_2D^+ ($N_{tot}(N_2D^+)$) is evaluated to be $(5.4 \pm 0.3) \times 10^{12}$ cm^{-2}. The error on $N_{tot}(N_2D^+)$ is given by propagating the errors on the total optical depth and the FWHM line width. Our $N_{tot}(N_2D^+)$ is very close to that obtained by Crapsi et al. (2005) ($(4.3 \pm 0.6) \times 10^{12}$ cm^{-2}), who derived it from the $N_2D^+(2–1)$ data.

Upper limits to $N_{tot}(N^{15}ND^+)$ and $N_{tot}(^{15}NND^+)$ were obtained from the 3σ upper limits to the integrated intensity $3\sigma\sqrt{\Delta v \delta v}$ of the transitions, where σ is the rms noise of the spectra, Δv is the FWHM line width of the spectra, assumed to be the same as that of $N_2D^+(1–0)$, and δv is the velocity resolution. Assuming local thermal equilibrium, the 3σ intensity upper limits were converted into the column density upper limits using Eq. (A4) of Caselli et al. (2002b), which is valid for optically thin emission. T_{ex} is assumed to be 5 K. We obtain $N_{tot}(N^{15}ND^+) < 7.0 \times 10^9$ cm^{-2} and $N_{tot}(^{15}NND^+) < 6.5 \times 10^9$ cm^{-2}.

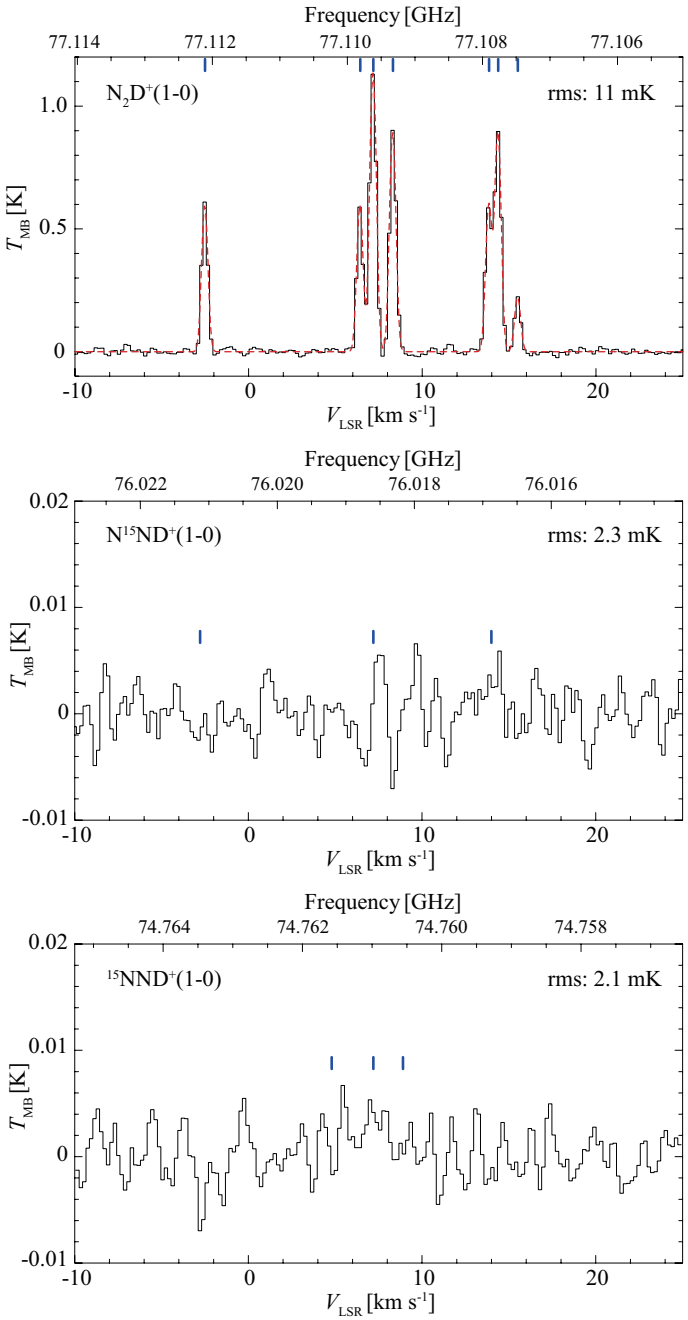

Fig. 1. Spectra of the N_2D^+(1–0) transition (*top panel*), the $N^{15}ND^+$(1–0) transition (*middle panel*), and the $^{15}NND^+$(1–0) transition (*bottom panel*) observed toward L1544. The intensity scale is the main-beam temperature. In the top panel, the red curve depicts the result of the HFS fit. The $N^{15}ND^+$(1–0) transition and the $^{15}NND^+$(1–0) transition were not detected down to 3σ levels in 0.2 km s^{-1} channels of 6.9 mK and 6.3 mK, respectively. The vertical blue lines indicate the positions of the expected hyperfine components.

4. Discussion and conclusion

From the column densities of the N_2D^+ isotopologs, we obtain the lower limits of the $^{14}N/^{15}N$ ratio of 730 for $N^{15}ND^+$ and 780 for $^{15}NND^+$. These lower limits are significantly higher than $[^{14}N/^{15}N]_{elem}$ in the local ISM (~200–300; Lucas & Liszt 1998; Ritchey et al. 2015). It is reasonable to consider the $^{14}N/^{15}N$ ratios of N_2D^+ as the ratio of N_2, because N_2D^+ primary forms by $N_2 + X_2D^+$, where X is H or D. Then our observations indicate that N_2 is significantly depleted in ^{15}N in the central part of L1544. If we assume T_{ex} of 4.5 K (5.5 K) in the column density evaluation, the lower limits of the $^{14}N/^{15}N$ ratios become 600 (950) for $N^{15}ND^+$ and 640 (1010) for $^{15}NND^+$. Our qualitative conclusion is thus robust against the assumed value of T_{ex}. Colzi et al. (2018) recently derived the $[^{14}N/^{15}N]_{elem}$ ratio in the local ISM of ~400 from the observations of HCN isotopologs toward a sample of 66 cores in massive star-forming regions. Even when this higher elemental abundance ratio is adopted, our qualitative conclusion does not change.

As described in Sect. 1, nitrogen isotope exchange reactions make N_2 enriched in ^{15}N; they are thus not relevant to the observed fractionation. Isotope-selective photodissociation of N_2 by penetrating interstellar FUV photons is also ruled out as the cause of the ^{15}N depletion because the penetration would be negligible in the central part of L1544, where N_2D^+ emission arises. Our lower limits of the $^{14}N/^{15}N$ ratios for N_2D^+ are consistent with those of N_2H^+ (~1000) obtained by Bizzocchi et al. (2013), which also supports that isotope-selective photodissociation of N_2 is not responsible for the ^{15}N depletion, as discussed in Sect. 1. We note that cosmic-ray induced photodissociation of N_2 does not cause ^{15}N fractionation because the destruction of N_2 by He^+ is much faster (Heays et al. 2014; Furuya & Aikawa 2018). Therefore, in situ chemistry is probably not responsible for the ^{15}N depletion in N_2 in the central part of L1544.

The most likely explanation is that the ^{15}N depletion is inherited from more diffuse gas, as recently proposed by Furuya & Aikawa (2018), based on their astrochemical models in forming and evolving molecular clouds. They found that during the evolution of molecular clouds, the nitrogen isotopes can be differentially partitioned between gas and ice, making ^{15}N-depleted gas and ^{15}N-enriched ice. In the molecular cloud, where the external UV radiation field is not fully shielded, $^{14}N^{15}N$ is selectively photodissociated with respect to $^{14}N_2$, which results in the enrichment of ^{15}N in the photodissociation product, atomic N. Atomic N is adsorbed onto grain surfaces and converted into NH_3 ice by surface reactions, while adsorbed N_2 does not react with other species, including atomic H. As long as the nonthermal desorption (especially photodesorption in their models) of NH_3 ice is less efficient than that of N_2 ice, the net effect is the loss of ^{15}N from the gas phase, producing ^{15}N-depleted gas and ^{15}N-enriched ice. When the external UV radiation field is sufficiently shielded, ^{15}N depletion does no longer proceed, but is largely conserved unless a significant amount of NH_3 ice is sublimated.

As noted by Furuya & Aikawa (2018), the mechanism is the most efficient around the chemical transition from atomic N to N_2, where the self-shielding of $^{14}N_2$ becomes important. Before the transition, both $^{14}N_2$ and $^{14}N^{15}N$ are efficiently photodissociated, while after the transition, the abundance of atomic N is too low to affect the bulk gas isotopic composition. Therefore, if the mechanism proposed by Furuya & Aikawa (2018) was at work in the parent cloud of L1544 or the outer regions of L1544, it means that the transition from atomic to molecular nitrogen should have occurred there as well.

Nitrogen chemistry mainly consists of three competing processes: (i) the conversion of atomic N to N_2 in the gas phase, (ii) destruction of N_2, for instance, via photodissociation and reaction with He^+, and (iii) freeze-out of atomic N and N_2 onto dust grains followed by surface reactions (e.g., Daranlot et al. 2012; Li et al. 2013). The conversion of atomic N into N_2 has been proposed to occur by slow neutral-neutral reactions, such as NO + N and CN + N (Herbst & Klemperer 1973; Daranlot et al. 2012). According to the pseudo-time-dependent gas-phase

astrochemical model under dense cloud conditions (10^4 cm^{-3}, 10 K, 10 mag) by Le Gal et al. (2014), the conversion of atomic N into N_2 takes an order of Myr, depending on assumed elemental abundances. In the gas-ice model of Daranlot et al. (2012), under the similar physical conditions, the conversion of atomic N to N_2 takes $\sim 5 \times 10^5$ yr, and it occurs after the significant fraction of nitrogen is frozen out. On the other hand, N_2 mainly forms via the reactions $NH_2 + N$ and $NH + N$ around the transition from atomic to molecular nitrogen in the models of Furuya & Aikawa (2018) and Furuya & Persson (2018), in which the dynamical evolution of molecular clouds is considered. NH_2 and NH are mainly formed via photodesorption of NH_3 ice, followed by photodissociation in the gas phase. In this case, the formation rate of N_2 from atomic N is, roughly speaking, similar to the freeze-out rate of atomic N. Considering that interstellar ices, at least water ice, are already abundant in molecular clouds with relatively low line-of-sight visual extinction (e.g., $\sim$3 mag for the Taurus dark clouds, Whittet 1993), it may not be surprising that the transition from atomic to molecular nitrogen occurs in the parent cloud of L1544 or in the outer regions of L1544. It should be noted that the N_2-dominant region could be larger than the regions traced by N_2H^+ and NH_3 emission, since their abundances are controlled not only by N_2, but also by CO; the catastrophic CO freeze-out, which occurs in the late stage of the interstellar ice formation at high densities ($\gtrsim 10^5$ cm^{-3}; e.g., Pontoppidan 2006), causes their abundances to be enhanced (e.g., Aikawa et al. 2005).

It may be interesting to estimate the partitioning of elemental nitrogen between gas and ice. The abundance of gaseous N_2 in dense prestellar cores was previously estimated from the comparison of N-chemistry models with the observations of N_2H^+ and other relevant species. Maret et al. (2006) inferred that gaseous N_2 contains only a few percent of the overall elemental nitrogen (N/H $= 6 \times 10^{-5}$ in the local ISM; Przybilla et al. 2008) in the dense cloud B68. Pagani et al. (2012) also inferred that gaseous N_2 contains $\lesssim$1% of elemental nitrogen in the prestellar core L183. While Maret et al. (2006) suggested that atomic N is the primary form of elemental nitrogen in B68 to account for this low gaseous N_2 abundance, their model predicts that NH_3 ice is the primary nitrogen reserver (see also Daranlot et al. 2012; Furuya & Persson 2018). The gas-ice astrochemical model by Ruaud et al. (2016), on the other hand, predicts that the HCN ice is more abundant than NH_3 ice. Figure 2 shows the fraction of elemental nitrogen in the form of ice as functions of the $^{14}N/^{15}N$ ratio of the bulk ice. In the figure, the $^{14}N/^{15}N$ ratio of the bulk gas (i.e., that of N_2) is assumed to be 1000. If NH_3 and HCN ices are the primary forms of elemental nitrogen in L1544, as predicted by the astrochemical models, the $^{14}N/^{15}N$ ratio of the icy species should be close to but slightly lower than $[^{14}N/^{15}N]_{elem}$.

Gérin et al. (2009) found that the $^{14}N/^{15}N$ ratio of gaseous NH_2D is >700 in L1544. The $^{14}N/^{15}N$ ratios of gaseous NH_3 in the cold gas of dense molecular clouds were derived to be 334 ± 50 in Barnard 1 and 340 ± 150 in NGC 1333 (Lis et al. 2010). These measurements indicate that gaseous NH_3 in the cold gas is not significantly enriched in ^{15}N. It should be noted, however, that the origin of gaseous NH_3 in the cold gas, that is, whether it is formed by gas-phase reactions or released from ices via nonthermal desorption, remains unclear. The $^{14}N/^{15}N$ ratio of icy species in star-forming regions could be constrained by measuring the molecular $^{14}N/^{15}N$ ratios in the warm ($\gtrsim$100 K) gas surrounding protostars. This type of observations is crucial for better understanding the nitrogen partitioning.

Finally, observations of comets have found that cometary NH_3 and HCN are enriched in ^{15}N by a factor of around three (Mumma & Charnley 2011; Shinnaka et al. 2016) compared to the Sun ($\sim$150 versus 441; Marty et al. 2011). The ammonia abundance with respect to water in cometary ices (0.4–1.4%) is lower than that in interstellar ices (typically $\sim$5%) (Mumma & Charnley 2011; Öberg et al. 2011). These (possible) differences between the N-bearing species in cometary and interstellar ices might indicate a primordial variation in the ice formation environments or ice processing in the solar nebula (e.g., Lyons et al. 2009; Furuya & Aikawa 2014).

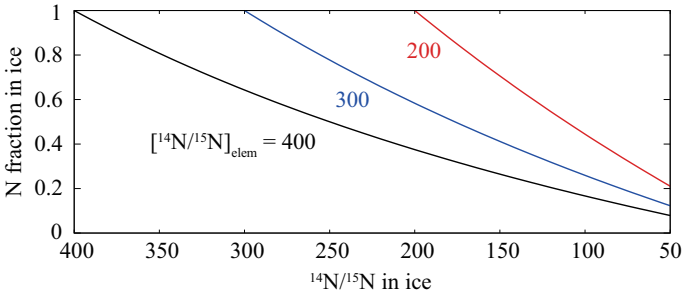

Fig. 2. Estimated fraction of elemental nitrogen in ices as functions of the $^{14}N/^{15}N$ ratio of the ices. The estimated fractions with different $[^{14}N/^{15}N]_{elem}$ are shown by different colors. In all cases, the $^{14}N/^{15}N$ ratio of the bulk gas is assumed to be 1000.

Acknowledgements. We are grateful to the IRAM staff for excellent support. We thank Yuto Sato for his help in preparing for the IRAM proposal, and we also thank the anonymous referee for useful comments that helped to improve this paper. This work is partly supported by JSPS KAKENHI Grant Numbers 16K17657 and 17K14245.

References

Aikawa, Y., Herbst, E., Roberts, H., & Caselli, P. 2005, ApJ, 620, 330
Bergin, E. A., & Tafalla, M. 2007, ARA&A, 45, 339
Bizzocchi, L., Caselli, P., & Dore, L. 2010, A&A, 510, L5
Bizzocchi, L., Caselli, P., Lenardo, E., & Dore, L. 2013, A&A, 555, 109
Caselli, P., Walmsley, C. M., Zucconi, A., et al. 2002a, ApJ, 565, 331
Caselli, P., Walmsley, C. M., Zucconi, A., et al. 2002b, ApJ, 565, 344
Charnley, S. B., & Rodgers, S. D. 2002, ApJ, 569, L133
Colzi, L., Fontani, F., & Rivilla, V. M., 2018, MNRAS, 976
Crapsi, A., Caselli, P., Walmsley, C. M., et al. 2005, ApJ, 619, 379
Daranlot, J., Hincelin, U., Bergeat, A., et al. 2012, PNAS, 109, 10233
De Simone, M., Fontani, F., Codella, C., et al. 2018, MNRAS, 476, 1982
Dore, L., Bizzocchi, L., Degli Esposti, C., & Tinti, F. 2009, A&A, 496, 275.
Furuya, K., & Aikawa, Y. 2014, ApJ, 790, 97
Furuya, K., & Aikawa, Y. 2018, ApJ, 857, 105
Furuya, K., & Persson, M. V. 2018, MNRAS, 476, 4994
Gérin, M., Marcelino, N., Biver, N., et al. 2009, A&A, 498, L9
Heays, A. N., Visser, R., Gredel, R., et al. 2014, A&A, 562, 61
Herbst, E., & Klemperer, W. 1973, ApJ, 185, 505
Hily-Blant, P., Bonal, L., Faure, A., & Quirico, E. 2013a, Icarus, 223, 582
Hily-Blant, P., Pineau des Forêts, G., Faure, A., Le Gal, R., & Padovani, M. 2013b, A&A, 557, 65
Lefloch, B., Bachiller, R., Ceccarelli, C., 2018, MNRAS
Le Gal, R., Hily-Blant, P., Faure, A., et al. 2014, A&A, 562, 83
Li, X., Heays, A. N., Visser, R., et al. 2013, A&A, 555, 14
Lis, D. C., Wootten, A., Gerin, M., & Roueff, E. 2010, ApJ, 710, L49
Lucas, R., & Liszt, H. 1998, A&A, 337, 246
Lyons, J. R., Bergin, E. A., Ciesla, F. J., et al. 2009, Geochim. Cosmochim. Acta, 73, 4998
Maret, S., Bergin, E. A., & Lada, C. J. 2006, Nature, 442, 425
Marty, B., Chaussidon, M., Wiens, R. C., Jurewicz, A. J. G., & Burnett, D. S. 2011, Science, 332, 1533
Müller, H. S. P., Thorwirth, S., Roth, D. A., & Winnewisser, G. 2001, A&A, 370, L49
Müller, H. S. P., Schlöder, F., Stutzki, J., & Winnewisser, G. 2005, JMoSt, 742, 215
Mumma, M., & Charnley, S. B. 2011, ARA&A, 49, 471
Öberg, K. I., Boogert, A. C. A., Pontoppidan, K. M., et al. 2011, ApJ, 740, 109

Pagani, L., Bourgoin, A., & Lique, F. 2012, A&A, 548, L4
Pety, J. 2005, in SF2A-2005 Conf. Ser., eds. F. Casoli, T. Contini, J. Hameury, & L. Pagani (EDP Sciences), 721
Pontoppidan, K. M. 2006, A&A, 453, L47
Przybilla, N., Nieva, M.-F., & Butler, K. 2008, ApJ, 688, L103
Redaelli, E., Bizzocchi, L., Caselli, P., 2018, A&A, in press, DOI: 10.1051/0004-6361/201833065
Ritchey, A. M., Federman, S. R., & Lambert, D. L. 2015, ApJ, 804, L3
Roueff, E., Loison, J. C., & Hickson, K. M. 2015, A&A, 576, 99
Ruaud, M., Wakelam, V., & Hersant, F. 2016, MNRAS, 459, 3756
Shinnaka, Y., Kawakita, H., Jehin, E., et al. 2016, MNRAS, 462, 195
Spezzano, S., Bizzocchi, L., Caselli, P., Harju, J., & Brünken, S. 2016, A&A, 592, L11
Terzieva, R., & Herbst, E. 2000, MNRAS, 317, 563
Whittet, D. C. B. 1993, in Dust and Chemistry in Astronomy (Bristol and Philadelphia: Institute of Physics Publishing), 9
Wirström, E. S., & Charnley, S. B. 2018, MNRAS, 474, 3720

Appendix A: Additional table

Table A.1. Hyperfine frequencies for $J = 1$–0 transitions of $N^{15}ND^+$ and $^{15}NND^+$ taken from Dore et al. (2009).

Species	F'–F	Frequency (GHz)	Relative intensity
$N^{15}ND^+$	1–1	76.0168733	1.000
	2–1	76.0185970	1.667
	0–1	76.0211239	0.333
$^{15}NND^+$	1–1	74.7605619	1.000
	2–1	74.7609788	1.667
	0–1	74.7615650	0.333